KH-TFMDI, a novel sirtuin inhibitor, alters the cytoskeleton and mitochondrial metabolism promoting cell death in *Leishmania amazonensis*

Brunno Renato Farias Verçoza,[a,b,c] Joseane Lima Prado Godinho [a,c], Sara Teixeira de Macedo-Silva [a,c], Kilian Huber,[d,e] Franz Bracher,[d] Wanderley de Souza[a,c,f] and Juliany Cola Fernandes Rodrigues[a,b,c,f#]

[a] Laboratório de Ultraestrutura Celular Hertha Meyer, Instituto de Biofísica Carlos Chagas Filho, Universidade Federal do Rio de Janeiro, Rio de Janeiro, Brazil

[b] Núcleo Multidisciplinar de Pesquisa em Biologia (NUMPEX-BIO), Polo Avançado de Xerém, Universidade Federal do Rio de Janeiro, Duque de Caxias, Brazil

[c] Instituto Nacional de Ciência e Tecnologia de Biologia Estrutural e Bioimagem, Rio de Janeiro, Brazil

[d] Departament of Pharmacy, Center for Drug Research, Ludwig-Maximilians-University, Munich, Germany

[e] Nuffield Department of Medicine, University of Oxford, United Kingdom

[f] Instituto Nacional de Metrologia, Qualidade e Tecnologia, Inmetro, Rio de Janeiro, Brazil

[#]Address correspondence to
Juliany Cola Fernandes Rodrigues,
email: juliany.rodrigues@xerem.ufrj.br
Laboratório de Ultraestrutura Celular Hertha Meyer
Instituto de Biofísica Carlos Chagas Filho
Universidade Federal do Rio de Janeiro
Av. Carlos Chagas Filho, 373
Cidade Universitária, CCS, Bloco G, subsolo
Rio de Janeiro, Brazil
CEP: 21941-902
Tel: +55 21 3938-6593
Fax: +55 21 2260-2364

Running title: Effects of KH-TFMDI on *Leishmania amazonensis*

Abstract

Treatment of leishmaniasis involves the use of antimonials, miltefosine, amphotericin B or pentamidine. However, the side effects of these drugs and the reports of drug-resistant parasites demonstrate the need for new treatments that are safer and more efficacious. Histone deacetylase inhibitors are a new class of compounds with potential to treat leishmaniasis. Herein, we evaluated the effects of KH-TFMDI, a novel histone deacetylase inhibitor, on *Leishmania amazonensis* promastigotes and intracellular amastigotes. The IC_{50} values of this compound for promastigotes and intracellular amastigotes were 1.976 μM and 1.148 μM, respectively, after 72h of treatment. Microscopic analyses revealed that promastigotes became elongated and thinner in response to KH-TFMDI, indicating changes in cytoskeleton organization. Immunofluorescence microscopy, western blotting and flow cytometry using an anti-acetylated tubulin antibody revealed an increase in the expression of acetylated tubulin. Furthermore, transmission electron microscopy revealed several ultrastructural changes, such as (a) mitochondrial swelling, followed by the formation of many vesicles inside the matrix; (b) presence of lipid bodies randomly distributed through the cytoplasm; (c) abnormal chromatin condensation; and (d) formation of blebs on the plasma membrane. Physiological studies for mitochondrial function, flow cytometry with propidium iodide and TUNEL assay confirmed the alterations in the mitochondrial metabolism, cell cycle, and DNA fragmentation, respectively, which could result to cell death by mechanisms related to apoptosis-like. All these together indicate that histone deacetylases are promising targets for the development of new drugs to treat *Leishmania,* and KH-TFMDI is a promising drug candidate that should be tested *in vivo*.

Acknowledgement

Introduction.

Leishmaniasis is one of the most important neglected diseases, caused by protozoan parasites of the *Leishmania* genus. The disease is present in 98 countries worldwide, affecting approximately 2 million people, with high rate of morbidity and mortality [1]. It can be divided in five main clinical forms: cutaneous, mucocutaneous, diffuse cutaneous, visceral, and post-kala-azar dermal leishmaniases. In Brazil, *Leishmania amazonensis* is one of the species responsible for the cutaneous form of the disease, mainly found in the Amazon region. In some patients infected with *L. amazonensis*, the immune system fails to respond appropriately, and they develop diffuse cutaneous leishmaniasis, in which the lesions cover a large part of the body and the disease is completely resistant to all available treatments [2].

The first line of treatment for leishmaniasis involves the use of pentavalent antimonials, except in India. In cases of antimonial-resistant *Leishmania*, other compounds such as amphotericin B (deoxycholate or lipid formulation), pentamidine, or miltefosine are used, depending of the species, clinical manifestation, and/or country [1]. However, these drugs are frequently associated with numerous severe side effects and resistance cases [1]. Thus, there is an urgent need to develop new drugs or therapeutic regimens that are more effective, safe and accessible for leishmaniasis patients.

The superfamily of sirtuins is composed of numerous proteins that are classified into at least four classes, class I - IV, in different organisms [3]. The proteins of this family are NAD+-dependent protein lysine deacetylases, which are important regulators of a variety of biological processes [3]. Several studies have demonstrated that sirtuins catalyze NAD+-dependent ε–N-acetyl-lysine deacetylation of both histones and non-histone proteins [3], thereby regulating many proteins involved in processes that are critical for cellular/organism survival, such as gene transcription, chromatin assembly, cell-cycle progression, apoptosis, DNA repair, energy production, metabolism and intracellular signaling [4]. Sirtuins are highly conserved proteins present in organisms ranging from bacteria to human and were recently found in protozoan parasites such as *Plasmodium*, *Trypanosoma* and *Leishmania* [5]. In *Leishmania*, several studies have demonstrated the presence of a gene encoding for a cytoplasmic protein termed *Leishmania infatum* SIR2-related protein 1 (LiSIR2RP1), a member of the silent information regulator 2 (SIR2) family, which includes proteins involved in cell survival, control of cell death and virulence [6-8]. The SIR2rp3 was also identified in *L. braziliensis* during a molecular modeling study using known and natural sirtuin inhibitors [9]; in this study, the authors also demonstrated that SIR2rp3 has strong analogy with

3

the mitochondrial human SIRT5 in terms of binding mode and interaction strength. Recently, sirtuins have been considered as potential targets for cancer therapies due to their critical roles in several biological processes, and HDAC inhibitors represent a structurally diverse group of compounds that inhibit histone deacetylation [10]. Thus, HDAC inhibitors have presented potent activity against several types of cancers, resulting in cell cycle arrest and differentiation, and finally apoptosis of the tumor cells [10]. Previous studies have reported the effects of HDAC inhibitors on parasitic protozoa such as *Leishmania* sp., some of them acting as modulators of the immune system during the treatment [11,12], or directly against the parasite's sirtuin, thus resulting in apoptosis-like cell death of the promastigotes [13,14]. In addition, the effect of KH-TFMDI against *Trypanosoma cruzi* was recently demonstrated, resulting in a significant effect on its growth and ultrastructure [15]. In this study, we show that KH-TFMDI inhibits the proliferation of both *Leishmania amazonensis* promastigotes and intracellular amastigotes, inducing several alterations in the ultrastructure and in the expression of acetylated tubulin, resulting in parasite cell death by a mechanism that still remains obscure, however it is similar to apoptosis [16].

Materials and Methods.

Parasite. *Leishmania amazonensis* WHOM/BR/75/JOSEFA strain was used in this study. It was isolated in 1975 from a patient with diffuse cutaneous leishmaniasis by Dr. Cesar A. Cuba-Cuba (Brasilia University, Brazil) and kindly provided by the *Leishmania* Collection of the Instituto Oswaldo Cruz (Code IOCL 0071 - FIOCRUZ). The parasites were maintained after inoculation of metacyclic infective promastigotes at the base of the tail of Balb/C mice. Intracellular amastigotes were isolated from the lesions and then differentiated into promastigotes, which were maintained in M199 medium (Gibco®) supplemented with 10% of fetal bovine serum (Cultlab®) at 25 °C. Infective metacyclic promastigotes from cultures in stationary phase were used to infect murine macrophages to obtain intracellular amastigotes.

Drug. KH-TFMDI (6,7-dichloro-3-[4-(trifluoromethyl)benzylidene]indolin-2-one) is a member of the 3-arylideneindolin-2-one family [Figure 1] [17], which was previously synthesized to inhibit the human histone deacetylases (compound no. 13 in ref. 24). The compound was dissolved in dimethyl sulfoxide (DMSO) (Merck), and the maximum concentration of DMSO in the cultures did not exceed 0.5%, a

concentration that does not interfere with the growth of *Leishmania*. The KH-TFMDI solution was stored at -20 °C.

Antiproliferative effects on promastigotes and intracellular amastigotes. Growth curves of *L. amazonensis* promastigotes were initiated with an inoculum of 1.0×10^6 cells/mL in M199 culture medium supplemented with 10% fetal bovine serum. After 24 h of growth, different concentrations of KH-TFMDI (0.5; 1; 2; 3; 4; 5 μM) were added and the cells were cultured for 96 h, with the cell density calculated every 24 h by counting the number of cells in a Neubauer chamber using contrast phase light microscopy. For the intracellular amastigote assays, murine macrophages and parasites were obtained as published previously [18]. After 24 h of initial infection, different concentrations of KH-TFMDI (1; 2; 3; 5 μM) were added, and the medium with the drug was changed every day for 3 days. IC_{50} values were calculated using the Regression Wizard tool from Sigma Plot 10 (Systat Software).

Immunofluorescence microscopy. Control and drug-treated *L. amazonensis* promastigotes were collected and processed for immunofluorescence microscopy using two antibodies: (a) anti α-tubulin antibody (Sigma-Aldrich) to observe the subpellicular microtubules and (b) anti-acetylated tubulin antibody (Sigma-Aldrich) to observe the pattern of tubulin acetylation in the parasites. Cells were washed in 0.1 M PHEM buffer, pH 7.2 (25 mM $MgCl_2$, 35 mM KCl, 5 mM EGTA, 10 mM HEPES, 30 mM PIPES), fixed in 4% freshly prepared formaldehyde in the same buffer for 30 min and allowed to adhere to coverslips previously coated with 0.1 % poly-L-lysine (Sigma-Aldrich). Cells were permeabilized by incubating in acetone (Merck) for 5 min at -20 °C. Next, parasites were incubated in 50 mM ammonium chloride for 30 min and then in blocking buffer containing 3% BSA and 0.025% fish gelatin in PBS, pH 7.2, twice for 30 min. After blocking nonspecific antigenic sites, cells were incubated with one of the following monoclonal antibodies: anti-α-tubulin at a dilution of 1:800 or anti-acetylated tubulin at a concentration of 0.06 mg/mL for 1h. After incubation with primary antibodies, coverslips were washed three times in blocking buffer for 5 min each and then incubated with secondary antibody for 1h (anti-mouse Alexa-488 or Alexa-546, both diluted 1:400). Finally, parasites were incubated with 5 μg/mL Hoechst or DAPI for 10 min, mounted on glass slides with *n*-propyl-gallate, sealed, and observed under a Zeiss Axioplan epifluorescence microscope (for visualization of anti-acetylated tubulin labeling) and Leica DMI6000 B with 3D Deconvolution (for visualization of anti-tubulin labeling). Distance between

5

nucleus and kinetoplast was measured using the fluorescence images of Hoescht, where 100 cells were analyzed by the NIH Image J Software (National Institute of Health, NIH).

Electron microscopy. To analyze the cell morphology and ultrastructure, control and KH-TFMDI-treated cells were washed twice in PBS, pH 7.2, and fixed and post-fixed according to protocols previously published, with some differences in scanning (SEM) and transmission electron microscopy (TEM) [18]. In summary, for SEM, samples were adhered to the coverslips, dehydrated with ethanol, critical point dried, mounted on "stubs", sputtered with a thin gold layer and observed under a FEI Quanta 250 scanning electron microscope. For TEM, two procedures have been adopted; for routine electron microscopy the samples were dehydrated in increasing concentrations of acetone (30%, 50%, 70%, 90%, and 100%) and embedded in Epon. For cytochemistry analysis using ethanolic phosphotungstic acid (PTA) to label positively charged groups, samples were fixed as described above, and then dehydrated in increasing concentrations of ethanol (30%, 50%, 70%, 90% and 100%). Then, cells were incubated in a solution containing 2% phosphotungstic acid (Ted Pella®) in ethanol for 4 h at room temperature under stirring, and, finally, embedded in Epon. Ultrathin sections were stained with uranyl acetate and lead citrate and observed using a Zeiss 900 electron microscope. For morphometric analysis of the morphological alterations induced by KH-TFMDI on the promatigotes, 20 and 25 cells examined by scanning electron microscopy were measured using the Image-J Software (National Institute of Health, NIH). The following parameters were evaluated: 1) cell body area; 2) total cell length (from the posterior tip to the end of the flagellum in the anterior region); 3) cell body length; 4) flagellum length

Western blot analysis. The acetylation of tubulin was evaluated in the control and KH-TFMDI-treated promastigotes by western blotting. Parasites were collected and washed three times with PBS. Cell lysates were obtained by incubating the promastigotes in an SDS sample buffer (Tris HCl 0.5M pH 6.8, glycerol 10%, bromophenol blue 1%, SDS 2% and 10% ß-mercaptoethanol) and boiling for 5 min. Protein concentration was determined by using a Bio-Rad protein assay (Bio-Rad). Next, cell lysates at the protein concentration of 35 μg were separated in a 10% SDS-PAGE polyacrylamide gel. To determine the molecular weight of the samples analyzed, standard Multimark® Multi-Colored Standard (Molecular Probes® Invitrogen - Life Technologies Corporation) was used. Proteins were then transferred to membranes, which were incubated with the same two antibodies used for the immunofluorescence

microscopy: anti-α-tubulin (1:400 dilution) and anti-acetylated tubulin (at a concentration of 0.06 μg/mL). For both antibodies, cells were incubated for 1h. To visualize the proteins, an antimouse secondary antibody conjugated to the peroxidase enzyme (1:2,000 dilution; from an ECL Plus Kit (GE Healthcare Life Science) was used. Images were revealed using a photodocumenter storm, and results were analyzed and quantified using Image-J software (National Institutes of Health, NIH) and subjected to statistical analysis using Prism 4 (GraphPad software).

Flow cytometry analysis of the extent of acetylated tubulin. For better quantify the acetylation of tubulin, flow cytometry was also carried out with anti-acetylated tubulin using the following protocol: 1 mL of control and KH-TFMDI-treated parasites were washed in 0.1 M PHEM buffer, pH 7.2 (25 mM MgCl$_2$, 35 mM KCl, 5 mM EGTA, 10 mM HEPES, 30 mM PIPES), and then fixed in 4% freshly prepared formaldehyde in 0.1 M PHEM buffer, pH 7.2. After that, cells were permeabilized by incubating in 90% methanol (Merck) for 30 min on ice. Next, parasites were incubated in blocking buffer containing 5% BSA in 0.1 M PHEM buffer, pH 7.2, twice for 5 min. After blocking nonspecific antigenic sites, cells were incubated with monoclonal antibody anti-acetylated tubulin at a concentration of 0.06 mg/mL. After incubation with primary antibodies, cells were washed three times in blocking buffer and then incubated with secondary antibody anti-mouse Alexa-488 diluted 1:400. Finally, parasites were washed in 0.1 M PHEM buffer, pH 7.2 and then resuspended in 500 µL of PBS, pH 7.2. Subsequently, flow cytometry analysis was carried out in an Accuri C6 cytometer (Becton Dickinson, United States). Fifty thousand events were evaluated; then, data were plotted and subjected to statistical analysis using Prism 4 (GraphPad software).

Nile Red accumulation. Control and KH-TFMDI-treated promastigotes were washed three times in Hank's solution, and the cell density was calculated by counting the number of cells in a Neubauer chamber. Then, 1.0×10^7 cells were resuspended in 10 μg/mL Nile Red, a neutral lipid fluorescence probe, and incubated for 20 min at room temperature in the dark. Cells were then washed in Hank's solution and transferred to a 96-well black plate in a final volume of 200 μL. The quantification of Nile Red accumulation was performed in a Spectramax microplate reader (Molecular Devices) using wavelengths specific for the detection of neutral lipids: 485 nm for excitation and 538 nm for emission.

Analysis of cell viability. Cell viability of the promastigotes treated with KH-TFMDI was evaluated by two methods. In the first method, propidium iodide was used: 1 mL of control and treated cells was washed in PBS-glucose, pH 7.2 (phosphate buffered saline + 10 mM glucose), and then resuspended in 500 µL of 10 µM propidium iodide in the same buffer, followed by incubation for 5 min at 25 °C. As positive control, parasites without treatment were incubated with 0.5% Triton-X100 (Sigma-Aldrich) in PBS glucose, pH 7.2, for 5 min. Subsequently, flow cytometry analysis was carried out in an Accuri C6 cytometer (Becton Dickinson, United States). Fifty thousand events were evaluated; then, data were plotted and subjected to statistical analysis using Prism 4 (GraphPad software). In the second method, CellTiter 96® Aqueous MTS Assay (Promega, United States) were used (18). For that, promastigotes were cultured in M199 medium starting from a cell density of 1.0×10^6 cells/mL; after 24 h of growth, different concentrations of KH-TFMDI inhibitor (0.5, 1, 2, 3, 4 and 5 µM) were added to the cultures. Cell viability was measured at 24 h, 48 h and 72 h of treatment, when each group (untreated or treated) was transferred to 96-well plate in triplicate. MTS/PMS assay reaction was quantified by optical density measurement at 490 nm in a microplate reader and SpectraMax M_2/M_2^e spectrofluorometer (Molecular Devices, United States). As a negative control, parasites were fixed with 0.4% nascent formaldehyde for 10 min at room temperature before the incubation. Data were plotted and subjected to statistical analysis using Prism 4 (GraphPad software).

Oxidative stress evaluation. Oxidative stress induced by treatment with KH-TFMDI was evaluated using fluorescent probes such as CM-H₂DCFDA and MitoSOX Red (Molecular Probes). For both analyses, 1 mL of control and treated promastigotes were washed once in PBS-glucose, pH 7.2. Then, cells were resuspended in a solution containing 10 µM CM-H₂DCFDA in the same buffer or 5 µM MitoSOX in Hanks solution and incubated for 20 min at 25 °C. At the end of the incubation, cells were washed and resuspended in 500 µL of PBS-glucose, pH 7.2. As positive control, parasites without treatment were incubated with 0.5% hydrogen peroxide (Sigma-Aldrich) in PBS-glucose, pH 7.2, for 20 min before labeling with CM-H₂DCFDA or MitoSOX Red. For the labeling with CM-H₂DCFDA, control group was treated with 50 mM N-acetyl cysteine (NAC) for 20 min at 25 °C. As negative control for analysis using CM-H₂DCFDA, control and KH-TFMDI-treated parasites were incubated with 20 mM NAC in PBS-glucose, pH 7.2, for 20 min. After all the incubations, samples were analyzed by flow cytometry in an Accuri C6 cytometer (Becton Dickinson, United States); fifty thousand events were

evaluated, then the data were plotted and subjected to statistical analysis using Prism 4 (GraphPad software).

Evaluation of the mitochondrial transmembrane electric potential ($\Delta\Psi m$)**.** Mitochondrial transmembrane electric potential ($\Delta\Psi m$) of control and treated promastigotes was evaluated using the JC-1 fluorochrome (Molecular Probes, United States). Initially, cells were washed in PBS, pH 7.2, and resuspended in a mitochondrial reaction medium containing 125 mM sucrose, 65 mM KCl, 10 mM HEPES/K$^+$, pH 7.2, 2 mM propidium iodide (Pi), 1 mM MgCl$_2$ and 500 μM EGTA. Then, 1.0×10^7 parasites were incubated with 10 μg/mL JC-1 for 40 min at 25 °C, with readings made every minute using a microplate reader and spectrofluorometer SpectraMax M$_2$/M$_{2e}$ (Molecular Devices). After 36 min, 2 μM FCCP was added to abolish the $\Delta\Psi m$ sustained at the inner mitochondrial membrane by the respiratory chain. Relative $\Delta\Psi m$ was obtained by calculating the ratio between the reading at 590 nm and the reading at 530 nm (590:530 ratio). Results obtained from each triplicate were analyzed and subjected to statistical analysis using Prism 4 (GraphPad software); data shown in the figures are representative of these experiments.

Cell cycle analysis. For cell cycle analysis, 1 mL of control and treated promastigotes were washed three times in PBS, pH 7.2, followed by fixation in 0.5% nascent formaldehyde for 5 min. After fixation, cells were washed three times in PBS, pH 7.2, and resuspended in 200 μL of PBS; to each sample, 1.3 mL of 70% ethanol in cold PBS was added, followed by incubation for 30 min in an ice bath. After that, cells were washed two times with PBS, pH 7.2, resuspended in 500 μL solution containing 50 μM PI + 25 μg/mL RNAseA, and incubated for 30 min at 37 °C. Analyses were carried out by flow cytometry in an Accuri C6 cytometer (Becton Dickinson, United States); fifty thousand events were evaluated, and the data were plotted and subjected to statistical analysis using Prism 4 (GraphPad software).

Analysis of cell death by apoptosis. Apoptosis-like cell death induced by the treatment with KH-TFMDI was determined using APO-BrdU TUNEL Assay Kit™ (Invitrogen). For TUNEL analysis, 2.0×10^7 cells for the control group, and 1.0×10^7 cells for treated groups were washed three times in PBS pH 7.2, followed by fixation in 1% nascent formaldehyde for 15 min in an ice bath. Then, cells were washed three times in PBS pH 7.2 and resuspended in 500 μL of PBS pH 7.2 with subsequent addition of 5 mL of 70% ethanol n in cold PBS, followed by incubation for 30 min in an ice bath. The samples were stored at –20

°C for 18 h prior to performing the TUNEL assay in order to enhance the labeling. At the end of this time of incubation, DNA labeling solution was prepared by mixing 10 μL of reaction buffer, 0.75 μL of TdT enzyme, 8.0 μL of BrdUTP and 31.25 μL of dH$_2$O. Samples were then resuspended in 50 μL of the DNA labeling solution and incubated at 37 °C for 60 min with shaking every 15 min to keep the cells in suspension. After that, 1.0 mL of rinse buffer was added to each tube and the samples were centrifuged at 300g for 5 min; supernatants were removed by aspiration, and this step was repeated once. For labeling, a solution of antibody were prepared containing 5 μL of the Alexa Fluor 488 dye–labeled anti-BrdU antibody and 95 μL of rinse buffer. Finally, supernatants were removed, 100 μL of the antibody solution were added for each sample and they were incubated for 30 min at room temperature, protected from light. This last step was followed by the addition of 0.5 mL of the propidium iodide/RNase A in the staining buffer to each sample and incubated for an additional 30 min under the same conditions. Analyses were carried out by flow cytometry in an Accuri C6 cytometer (Becton Dickinson, United States); fifty thousand events were evaluated, then the data were plotted and subjected to statistical analysis using GraphPad Prism software (GraphPad Software).

Statistical analysis. The means and standard deviations were calculated for experiments performed in triplicate (except for experiments of optical microscopy and electron microscopy). A two-way ANOVA with Bonferroni post-test was used to analyze the antiproliferative effect, and the Tukey's test was used to the Nile Red accumulation. Different p values were obtained for each statistical analysis and they are mentioned in the legend of the figures.

Results.

Antiproliferative effects. The antiproliferative effects of KH-TFMDI on promastigotes and intracellular amastigotes were evaluated. For both developmental stages, the effects were time- and concentration-dependent, with the most potent effect observed on the last day of treatment [72 h] (Fig. 2A-B). Table 1 shows that KH-TFMDI was effective for both developmental stages, presenting activity in a concentration range between 1 and 5 μM. The IC$_{50}$ values were obtained for 24, 48 and 72 h of treatment and they are summarized in the Table 1. Intracellular amastigotes were more susceptible after 72 h of treatment presenting an IC$_{50}$ value of 1,148 μM. On the other hand, promastigotes were slightly more resistant than amastigotes, with an IC$_{50}$ value of 1,976 μM. During the treatment of infected macrophages,

10

no cytotoxicity effects on the host cells were observed, confirming results obtained previously with mammalian cells [15].

Effects of KH-TFMDI on cell morphology and expression of acetylated-tubulin. To better understand the morphological changes induced by KH-TFMDI in promastigotes, we used three different techniques: 1) Phase contrast light microscopy and immunofluorescence with 3D Deconvolution; 2) Scanning electron microscopy; and, 3) Morphometric analysis. For immunofluorescence assays two different antibodies were used: anti-α-tubulin, and anti-acetylated tubulin. After 48 h of treatment, the shape of promastigotes changed significantly in response to KH-TFMDI. The parasites became thinner and longer (Fig. 3). The morphological changes were even more evident when the parasites are observed after 3D deconvolution of immunofluorescence images obtained for anti-α-tubulin labeling (Fig. 3). The morphological changes in the cell body were confirmed by scanning electron microscopy, which also revealed alterations on the cell surface. Figure 4A shows a control promastigote with a normal shape and no cell surface alterations. After treatment with 3 or 5 μM KH-TFMDI for 48 h, the promastigotes became thinner and elongated (Fig. 4B-D), as observed previously by light microscopy; however, several cells were dilated at the central/anterior region of the body, most likely where the nucleus is located (Fig. 4E, arrowhead). In addition, blebs were observed at the surface of the cell body (Fig. 4C, D, F, arrows). To quantify the morphological alterations on the cell body of promastigotes submitted to treatment with KH-TFMDI, morphometric analyses were carried out from images obtained by scanning electron microscopy and fluorescence microscopy of Hoescht-labeled cells. Trying to describe all the alterations observed, five patterns of measure were chosen: 1) cell body area, which means only the area of cell body without include the flagellum; 2) total cell lenght; 3) cell body length; 4) length of the flagellum, where the measurement was done from the basis of flagellum inserted at the flagellar pocket to its tip; and, 5) distance between nucleus and kinetoplast, in this case using the fluorescence images of Hoescht-labeled cells. Figures 5A-D shows representative cells from scanning electron microscopy and fluorescence microscopy using Hoescht that was used in the morphometric analysis. In panels A and B, arrowheads and arrows point to cell body and flagellum; while in panels C and D, arrowheads point to distance between nucleus and kinetoplast. All the measurements are summarized in the Figure 5E-I. The treatment with KH-TFMDI induced a significant reduction of the cell body area (Fig. 5E), however promoted a significant increase in the length of the promastigotes (Fig. 5F), in the length of cell body

11

(Fig. 5G) and in the length of the flagellum (Fig. 5H). All these morphological changes resulted in a significant increase in the distance between nucleus and kinetoplast, which is evident in the images and confirmed by quantification (Fig. 5I). All these analysis confirmed the images observed by scanning electron microscopy and light microscopy. Figure 5J shows a table with the mean number of the measurements made for control and 5 μM KH-TFMDI, confirming the alterations observed in the cell morphology of promastigotes.

Trying to understand if the morphological changes of promastigotes and cytoskeleton remodeling were induced by possible alterations in acetylation of tubulin, immunofluorescence, western blotting and flow cytometry analysis were carried out using the anti-acetylated tubulin antibody. Figure 6 shows a concentration-dependent significant increase in the acetylation of tubulin, indicating that KH-TFMDI could be causing a hyperacetylation of tubulin. The increase in the expression of acetylated tubulin induced by incubation of promastigotes with KH-TFMDI was confirmed by western blotting, densitometry and flow cytometry analysis (Fig. 7A-I). The expression of α-tubulin was also investigated and its expression was not altered with the treatment (Fig. 7C, F), probably indicating that the remodeling of cytoskeleton and the morphological changes, which should be related to tubulin acetylation.

Ultrastructural effects of KH-TFMDI on promastigotes observed by electron microscopy. Scanning electron microscopy was used to better analyze the alterations in the cell morphology and cell surface of control and treated-promastigotes.

Transmission electron microscopy was used to analyze the ultrastructural alterations induced by KH-TFMDI. Figure 8A shows a control promastigote with a normal structural organization of the mitochondrion (M), nucleus (N), kinetoplast (k), flagellum (F) and cell surface. After treatment with KH-TFMDI, several alterations were observed. First, blebs were detected in the plasma membrane that covers the cell body (Fig. 8B-C, arrowhead). In some regions, a lipid body was observed in close association with the plasma membrane where the bleb was formed (Fig. 8B, arrow). The second noted change was the accumulation of lipid bodies near the plasma membrane, mitochondrion and endoplasmic reticulum profiles (Fig. 7D-E, arrows); some of the lipid bodies were eletronlucent and had an irregular shape (Fig. 7D, arrows), whereas others were eletrondense, with a high affinity to osmium tetroxide (Fig. 7E, arrows). At a higher concentration of KH-TFMDI (10 μM), the main alterations were noted in the mitochondrion, which presented with an intense swelling followed by a loss of the matrix content (Fig.

12

8D) and vesiculation of the inner mitochondrial membrane (Fig. 8E, arrowheads). The presence of cisternae of the endoplasmic reticulum involving parts of the cytoplasm, lipid bodies (arrows), and glycosome (arrowhead) were also detected (Fig. 9A). In addition, several secreted vesicles were observed inside the flagellar pocket (Fig. 9A, FP). At this concentration, ultrastructural alterations were also observed in the nucleus, which presented morphological phenotypes such as a total decondensation of the chromatin (Fig. 9B) or its fragmentation (Fig. 9C-F). In some of the images, the nucleus appeared swollen, contributing to the deformation of the cell body (Fig. 9D, small arrow), or closely associated with the plasma membrane (Fig. 9C, small arrow). Furthermore, a lipid body was observed touching the plasma membrane, suggesting cell lysis (Fig. 9E, arrow). Deformation of the cell body was also observed in Figure 9E (small arrow). It is interesting to note that in some of these images, a special correlation between the mitochondrion and lipid bodies was observed (Fig. 9D,F). Comparing these micrographs with those of the control promastigotes (Fig. 8A), the ultrastructure of the KH-TFMDI-treated parasites appears to be significantly changed.

To better analyze the DNA condensation, we performed a cytochemical staining for electron microscopy to reveal basic proteins (including histones) by the incubation with phosphotungstic acid (PTA). In control parasites (Fig. 10A), it is possible to observe a regular pattern of nuclear chromatin condensation, similar to that found in parasites post-fixed with osmium tetroxide (Fig. 8A). PTA cytochemistry confirmed the significant alterations in the DNA condensation after treatment with KH-TFMDI (Fig. 10A-D). Different patterns of condensation can be observed. Figure 10B shows a nucleus with the chromatin completely decompacted and the nuclear matrix appears eletronlucent (treatment with 5 µM KH-TFMDI). On the other hand, in Figs. 10C-D the pattern of condensation is different from the other images (10 µM KH-TFMDI). In Fig. 10C, the nuclear matrix presents regions containing less condensed chromatin, however in several areas the chromatin remains highly condensed (arrow). In addition, some cells presented an intense fragmentation of nuclear chromatin, a typical phenotype indicative of apoptosis-like cell death (Fig. 10D).

Evaluation of different cellular phenotypes induced by treatment: lipid bodies accumulation, cell viability, oxidative stress and mitochondrial function. The analysis of drug-treated cells by transmission electron microscopy revealed different ultrasctructural alterations such as: 1) accumulation of lipid bodies; 2) marked lesions in the mitochondrion; and 3) presence of phenotypes typically found in

apoptosis-like cell death. Thus, we decided to further characterize these effects investigating the accumulation of lipid bodies, cell viability, mitochondrial transmembrane electric potential ($\Delta\Psi m$), and oxidative stress induced by KH-TFMDI (Fig. 11A-H). First, we performed incubation with Nile Red, a fluorescence marker for neutral lipids, evaluating the accumulation of lipid bodies by fluorimetry. Results indicated a concentration-dependent increase of fluorescence intensity that means increase of Nile Red accumulation (Figure 11A), in close agreement with the observations made by electron microscopy that showed the presence of several lipid bodies in treated promatigotes. Second, we performed cell viability analysis using two distinct methodologies: 1) Evaluation of plasma membrane integrity using propidium iodide by flow cytometry (Fig. 11B), and 2) Evaluation of mitochondrial dehydrogenases activity using MTS/PMS assay (Fig. 11C). Both analyses revealed that cell viability reduced significantly after treatment with 5 µM KH-TFMDI for just 24 h. For plasma membrane integrity, the alterations in the percentage of viable promastigotes were observed just in the higher concentrations (4 and 5 µM) after 72 h of treatment [Fig. 11B]. However, for mitochondrial dehydrogenases all treatments induced reduction of viable cell population in a time and concentration-dependent manner (Fig. 11C). These analyses support the results obtained by electron microscopy, where several images indicated morphological alterations on the plasma membrane and mitochondrion.

Due to the alterations in the ultrastructure of the promastigote's mitochondrion and the significant reduction of cell viability demonstrated by MTS/PMS assay, we decided to evaluate in detail the effects of KH-TFMDI on some physiological functions including mitochondrial function, oxidative stress and cell death. The first analysis evaluated the cellular oxidative stress by measuring the levels of reactive oxygen species (ROS) using the fluorescent dye H_2DCFDA, which stains total levels of ROS produced by cells, including singlet oxygen, superoxide, hydroxyl radical and various peroxide and hydroperoxides. The results indicated that concentrations of 4 µM and 5 µM were able to increase significantly the levels of ROS after 24 h and 48 h of treatment (Fig. 11D). The effect was concentration and time-dependent. For 24 h, KH-TFMDI induced an increase of 7% and 14% in ROS production for the concentration of 4 µM and 5 µM KH-TFMDI, respectively (Fig. 11D); after 48 h, the effect was much more evident, with an increase of 20% and 30% in ROS production for the same concentrations, respectively (Fig. 11E). In order to mimic the ROS production induced by treatment and confirm the effect induced by KH-TFMDI, two different controls were used: H_2O_2 as a positive control, and N-acetyl cysteine (NAC) as a negative

14

control. Whilst H_2O_2 induced a potent increase in ROS production, NAC inhibited the production in drug-treated parasites restoring the levels close to parasites without treatment [Fig. 11D-E]. Due to the strong effect of KH-TFMDI in inducing oxidative stress in the treated promastigotes by increasing intracellular ROS associated with ultrastructural changes in the mitochondrion observed by electron microscopy, we decided to investigate the mitochondrial function using two parameters: 1) Production of mitochondrial superoxide by using a highly selective red indicator designed to detect exclusively this population of ROS, the MitoSOX Red; 2) Evaluation of the mitochondrial transmembrane electric potential ($\Delta\Psi m$) using the fluorophore JC-1. KH-TFMDI induced a significant dose-dependent increase of mitochondrial superoxide after 48 h of treatment (Fig. 11F). In the higher concentration of KH-TFMDI (5 µM), the increase became near to the effect induced by the NAC. Analysis of the mitochondrial transmembrane potential ($\Delta\Psi m$) confirmed the results of MitoSOX. $\Delta\Psi m$ was decreased by the treatment, which a significant effect mainly in the concentration of 5 µM TFMDI that was similar to the effect observed for the FCCP protonophore (Fig. 11G-H). The $\Delta\Psi m$ reduced during 25 min of reading and was completely abolished when FCCP was added (Fig. 11H), confirming the potent effect of KH-TFMDI in the mitochondrial function.

Cell cycle analysis. To confirm possible alterations in the cell cycle induced by treatment of promastigotes with KH-TFMDI, we incubated the parasites with propidium iodide and analyzed by flow cytometry. For all times of incubation in presence of KH-TFMDI, the cell cycle arrest on G0/G1 phase (Fig. 12A-C) and the percentage of inhibition was significant in the higher concentrations (4 and 5 µM). After 48 h, a slow increase in a concentration-dependent manner in the percentage of sub-G0 population was observed (Fig. 12B, arrow). Furthermore, after 72 h increased significantly the percentage of cells in G0/G1 phase, and also in sub-G0 that means cells undergoing cell death (Fig. 12C). On the other hand, we also observed a decrease in the G2/M for the higher concentration (5 µM) [Fig. 12C]. It is also interesting to compare the S phase between the different times of treatment (24, 48, and 72 h). There was a significant reduction in the percentage of cells in this phase, confirming the accumulation of cells in sub-G0 and G0/G1 phases (Fig. 12A-C, arrowheads).

Analysis of DNA fragmentation induced by treatment of promastigotes with KH-TFMDI. All previous results indicated that cells are undergoing cell death by necrosis (PI positive) or apoptosis-like (based on analysis of transmission electron microscopy). To confirm this last phenotype, we performed

15

APO-BrdU TUNEL assay to evaluate the DNA fragmentation. After 48 h of treatment, the percentage of cells undergoing DNA fragmentation increased from 16,1% observed in control promastigotes to 77% in parasites treated with 3 μM KH-TFMDI (Fig. 13A-E). For 4 and 5 μM KH-TFMDI, the increase in DNA fragmentation was higher, however no significant variation was observed between them (Fig. 3D-E). On the other hand, for 10 μM TFMDI there was a significant decrease that can be related to the physiological state of the parasites, where several cells are completely destroyed (Fig. 13F).

Discussion.

Several recent studies have demonstrated the presence of class III histone deacetylases (HDACs or sirtuin-related proteins) in *Leishmania* [6,8], and some of them reported the development of new HDAC inhibitors for use against different types of tumors [10]. These studies point to histone deacetylases as a potential new drug target. Therefore, we decided to investigate the effects of a novel HDAC inhibitor, KH-TFMDI, on *Leishmania amazonensis*.

Our results indicate that KH-TFMDI has a significant antiproliferative effect against both promastigotes and intracellular amastigotes with IC_{50} values of 2 μM and 1 μM, respectively. Compared with other compounds, including some of those that are currently used for the treatment of leishmaniasis, these IC_{50} values indicate that KH-TFMDI should be considered as a potential treatment for leishmaniasis. For example, several reports have shown that the IC_{50} for miltefosine varies between 15 and 25 μM, depending on the *Leishmania* species [18]. In our model of *L. amazonensis* cultivation, the IC_{50} found for miltefosine was around 25 μM for promastigotes and 20 μM for intracellular amastigotes (data not shown). Thus, KH-TFMDI was more potent than miltefosine (Table 1). Against *Trypanosoma cruzi,* a recent study showed IC_{50} values similar to those obtained here for *Leishmania*, with a low level of cytotoxicity for mammalian cells *in vitro* [15], where it was demonstrated that for macrophages the CC_{50} was 81 μM. Thus, KH-TFMDI was more selective for the parasites than mammalian host cells. Trying to understand the biological activity of KH-TFMDI on *L. amazonensis*, we used several techniques such as light and electron microscopy, SDS-page and western blotting, flow cytometry and fluorimetry.

Effects on cell shape. Light and electron microscopy showed that the cell body shape of the promastigotes was completely altered at low concentrations of KH-TFMDI. After just 24 h of incubation, parasites became swollen in the medial and anterior regions of the cell body, where the nucleus is located.

16

However, after 48 h of treatment, promastigotes became thinner and longer. Morphometric analysis using images obtained by scanning electron microscopy confirm these alterations, and also demonstrated that changes in cell morphology result in the repositioning of intracellular organelles such as the nucleus and kinetoplast. The distance between them increased significantly. Furthermore, transmission electron microscopy indicated that the swelling of the cell body could be related to the morphological changes in the nucleus. On the other hand, immunoblotting and immunofluorescence analyses showed that KH-TFMDI was able to promote a hyperacetylation of tubulin, which was concentration-dependent. Tubulin acetylation has some important functions for the eukaryotic cell; one is related to the increase of microtubule stability. In addition, motor proteins like kinesins have more affinity for acetylated tubulin, resulting in an increase of vesicular traffic [19]. Besides, it has been demonstrated in mammalian cells that proteins from the sirtuin 2 protein (SIRT2) family can interact with HDAC6, a typically cytoplasmic class II histone deacetylase enzyme, which regulates the dynamic instability of the microtubules by tubulin acetylation [20]. It is possible that the treatment of *L. amazonensis* with KH-TFMDI produces a synergic effect in the inhibition of SIRT2 and HDAC6, resulting in an increase in the expression of acetylated tubulin. The tubulin acetylation process was demonstrated in *L. infantum* when a protein with functional homology to SIRT2, LiSIR2RP1, was identified [8]. The tubulin hyperacetylation induced by KH-TFMDI could lead to the remodeling of the subpelicullar microtubules, thus resulting in a dramatic alteration of the cell body shape. Interestingly, the presence of lipid bodies in close association with the subpellicular microtubules and plasma membrane could explain the protrusions observed in the parasite surface. However, some of these protrusions could also be blebs that can occur during apoptosis-like cell death. KH-TFMDI also caused an increase of at least 2-fold in the distance between the nucleus and kinetoplast in promastigotes. This is consistent with the remodeling of the cytoskeleton being promoted by tubulin hyperacetylation. The alterations on cell morphology and cytoskeleton remodeling were not carry out in intracellular amastigotes, because it is special hard to work with the intracellular developmental stage; however, we have plan to continue the studies with this class of compounds, and some new experiments will be designed to observe how the treatment may affect the parasite that lives inside the parasitophorous vacuole.

Lipid accumulation. Another effect of KH-TFMDI is the random accumulation of lipid bodies throughout the cytoplasm. Interestingly, the lipid bodies had distinct morphologies related to their sizes,

shape and electron density; these differences could be due to different lipid compositions acquired during the treatment. Several studies have described the role of sirtuins in cellular metabolism as being related to the accumulation and degradation of lipid in different cell types [3,21,22]. Recently, a mammalian mitochondrial SIRT4 was described [23] that is important in coordinating the balance between lipid synthesis and catabolism, promoting lipogenesis and inhibiting fatty acid oxidation. We believe that KH-TFMDI could inhibit a sirtuin, most likely one that is homologous to the mammalian SIRT4 and has not yet been described in *Leishmania,* thus resulting in the accumulation of aberrant lipid bodies.

Effects of KH-TFMDI on cell viability, oxidative stress and mitochondrial function. To evaluate possible mechanisms of action of KH-TFMDI against promastigotes, we used several approaches to study the physiological effects induced by treatments. First of all, we evaluated the cell viability using two methods: membrane integrity and MTS assay. The reduction in cell viability was caused by both, loss of membrane integrity and mitochondrial activity. Membrane integrity could be directly related to alterations in the subpellicular microtubules produced by hyperacetylation. Furthermore, sirtuins in higher eukaryotes are important for the mitochondrial activity and lipid metabolism [24]. KH-TFMDI also induced a collapse of the mitochondrial membrane potential and an increase in the production of reactive oxygen species and mitochondrial superoxide, resulting in an oxidative stress. Increase of mitochondrial superoxide may be related to inhibition of the enzyme superoxide dismutase A (SODA). A previous study demonstrated the important role of the iron-containing superoxide dismutase A enzyme (FeSODA2) in the development of resistance in cases of visceral leishmaniasis in India that could be related to the overexpression of SIR genes 2 [25]. Other studies have described the important role of sirtuins in regulating the activity of superoxide dismutase enzymes in mammals and therefore their key role in the regulation and maintenance of oxidative stress [26-28]. On the other hand, a recent study demonstrated the role of SIRT3 in the regulation of the major aspects of the cellular biology, including mitochondrial dynamics and ATP generation [29]. Thus, our results indicate that KH-TFMDI is specially affecting the cytoskeleton dynamics, mitochondrial function and lipid metabolism in treated promastigotes. Although other sirtuins have not been yet described in *Leishmania*, we believe that there are homologous proteins described in *Homo sapiens*, which may play similar roles in this organism, since it is a key class of proteins with several functions in higher eukaryotes.

Cell cycle and cell death analysis. Flow cytometry of propidium iodide-labeled promastigotes indicated an arrest of the cell cycle in the G1 phase with a concomitant decrease of the number of parasites in G2 and M phases, similar to results obtained in other studies [30,31]. In addition, an increase in the number of parasites in sub-G0 was also observed, indicating a nuclear DNA fragmentation. Furthermore, transmission electron microscopy revealed that treated promastigotes presented morphological alterations typically found in cells undergoing cell death, as previously observed in other eukaryotic cells treated with HDAC inhibitors [21,32,33]. During the treatment, promastigotes had varying levels of chromatin condensation (including decondensation and/or fragmentation), mitochondrial swelling and vesiculation of the inner mitochondrial membrane; all these morphological phenotypes are typically found during apoptosis-like cell death in *Leishmania* and other protozoan parasites. Herein, we confirmed a possible apoptosis-like death observed by electron microscopy, by TUNEL analysis and evaluation of the mitochondrial transmembrane potential ($\Delta\Psi m$). In higher eukaryotic cells, apoptosis induced by HDAC inhibitors is correlated with the inhibition of SIRT2 [34]. These effects could be related to the subcellular localization of SIRT2 in the nucleus, cytoplasm and mitochondrion as well as its other biological functions related to non-histone proteins [5]. SIRT2 is also involved in the regulation of p53-dependent cell death through its deacetylation [35]. The presence of proteins with homology to SIRT2 has been recently reported in *Leishmania;* however, their functions are not well known [5,6,8]. In *Leishmania*, KH-TFMDI may act by inhibiting sirtuins, thereby disrupting cell proliferation and survival, as has been established for other cell types. However, cell death in protozoan parasites still remains a controversy theme that requires further studies [16].

On the other hand, in KH-TFMDI-treated cells, transmission electron microscopy revealed the association of the endoplasmic reticulum with mitochondrion, lipid bodies and glycosomes, a phenotype that is typically found during autophagic processes, which have also been described in *Leishmania* sp. [36]. In eukaryotic cells, SIRT2 is also involved in the regulation of autophagy, interfering with lysosomal degradation of protein aggregates [37]. In *L. donovani*, a recent study demonstrated that the expression levels of SIRT2 are upregulated when the parasite is subjected to different chemotherapeutic treatments that exacerbate the autophagic process [38]. It is possible that by modulating the expression of SIRT2, KH-TFMDI leads to an increase in autophagosome formation and autophagy as an attempt to recycle damaged organelles.

In conclusion, KH-TFMDI can be considered as a new potential anti-*Leishmania* agent because it can inhibit the growth of intracellular amastigotes, the clinically relevant stage of *Leishmania*. KH-TFMDI also induces several changes in organelle physiology, general cell morphology and structural organization in parasites, resulting in phenotypes that are typically found in cells undergoing cell death and autophagy. We also demonstrated that KH-TFMDI can modulate the expression of acetylated-tubulin, resulting in a remodeling of the microtubule cytoskeleton. However, additional studies are necessary to define better the mechanisms of action and determine efficacy in animal models of leishmaniasis.

References.

1. Rodrigues JC, Godinho JL, de Souza W (2014) Biology of human pathogenic trypanosomatids: epidemiology, lifecycle and ultrastructure. Sub-cellular biochemistry 74:1-42. doi:10.1007/978-94-007-7305-9_1

2. Lainson R, Shaw JJ, Silveira FT, de Souza AA, Braga RR, Ishikawa EA (1994) The dermal leishmaniases of Brazil, with special reference to the eco-epidemiology of the disease in Amazonia. Memorias do Instituto Oswaldo Cruz 89 (3):435-443

3. Jing H, Lin H (2015) Sirtuins in epigenetic regulation. Chemical reviews 115 (6):2350-2375. doi:10.1021/cr500457h

4. Finkel T, Deng CX, Mostoslavsky R (2009) Recent progress in the biology and physiology of sirtuins. Nature 460 (7255):587-591. doi:10.1038/nature08197

5. Religa AA, Waters AP (2012) Sirtuins of parasitic protozoa: in search of function(s). Molecular and biochemical parasitology 185 (2):71-88. doi:10.1016/j.molbiopara.2012.08.003

6. Vergnes B, Sereno D, Madjidian-Sereno N, Lemesre JL, Ouaissi A (2002) Cytoplasmic SIR2 homologue overexpression promotes survival of Leishmania parasites by preventing programmed cell death. Gene 296 (1-2):139-150

7. Vergnes B, Vanhille L, Ouaissi A, Sereno D (2005) Stage-specific antileishmanial activity of an inhibitor of SIR2 histone deacetylase. Acta tropica 94 (2):107-115. doi:10.1016/j.actatropica.2005.03.004

8. Tavares J, Ouaissi A, Santarem N, Sereno D, Vergnes B, Sampaio P, Cordeiro-da-Silva A (2008) The Leishmania infantum cytosolic SIR2-related protein 1 (LiSIR2RP1) is an NAD+-dependent deacetylase and ADP-ribosyltransferase. The Biochemical journal 415 (3):377-386. doi:10.1042/BJ20080666

9. Sacconnay L, Smirlis D, Queiroz EF, Wolfender JL, Soares MB, Carrupt PA, Nurisso A (2013) Structural insights of SIR2rp3 proteins as promising biotargets to fight against Chagas disease and leishmaniasis. Molecular bioSystems 9 (9):2223-2230. doi:10.1039/c3mb70180h

10. Monneret C (2005) Histone deacetylase inhibitors. European journal of medicinal chemistry 40 (1):1-13. doi:10.1016/j.ejmech.2004.10.001

11. Silvestre R, Cordeiro-da-Silva A, Tavares J, Sereno D, Ouaissi A (2006) Leishmania cytosolic silent information regulatory protein 2 deacetylase induces murine B-cell differentiation and in vivo production of specific antibodies. Immunology 119 (4):529-540. doi:10.1111/j.1365-2567.2006.02468.x

12. Andrews KT, Haque A, Jones MK (2012) HDAC inhibitors in parasitic diseases. Immunology and cell biology 90 (1):66-77. doi:10.1038/icb.2011.97

13. Tavares J, Ouaissi A, Lin PK, Tomas A, Cordeiro-da-Silva A (2005) Differential effects of polyamine derivative compounds against Leishmania infantum promastigotes and axenic amastigotes. International journal for parasitology 35 (6):637-646. doi:10.1016/j.ijpara.2005.01.008

14. Tavares J, Ouaissi A, Silva AM, Lin PK, Roy N, Cordeiro-da-Silva A (2012) Anti-leishmanial activity of the bisnaphthalimidopropyl derivatives. Parasitology international 61 (2):360-363. doi:10.1016/j.parint.2011.11.005

15. Veiga-Santos P, Reignault LC, Huber K, Bracher F, W DES, TM DEC (2014) Inhibition of NAD+-dependent histone deacetylases (sirtuins) causes growth arrest and activates both apoptosis and autophagy in the pathogenic protozoan Trypanosoma cruzi. Parasitology 141:814-825. doi:10.1017/S0031182013001704

16. Proto WR, Coombs GH, Mottram JC (2013) Cell death in parasitic protozoa: regulated or incidental? Nature reviews Microbiology 11 (1):58-66. doi:10.1038/nrmicro2929

17. Huber K, Schemies J, Uciechowska U, Wagner JM, Rumpf T, Lewrick F, Suss R, Sippl W, Jung M, Bracher F (2010) Novel 3-arylideneindolin-2-ones as inhibitors of NAD+ -

dependent histone deacetylases (sirtuins). Journal of medicinal chemistry 53 (3):1383-1386. doi:10.1021/jm901055u

18. Godinho JL, Georgikopoulou K, Calogeropoulou T, de Souza W, Rodrigues JC (2013) A novel alkyl phosphocholine-dinitroaniline hybrid molecule exhibits biological activity in vitro against Leishmania amazonensis. Experimental parasitology 135 (1):153-165. doi:10.1016/j.exppara.2013.06.015

19. Hammond JW, Cai D, Verhey KJ (2008) Tubulin modifications and their cellular functions. Current opinion in cell biology 20 (1):71-76. doi:10.1016/j.ceb.2007.11.010

20. Nahhas F, Dryden SC, Abrams J, Tainsky MA (2007) Mutations in SIRT2 deacetylase which regulate enzymatic activity but not its interaction with HDAC6 and tubulin. Molecular and cellular biochemistry 303 (1-2):221-230. doi:10.1007/s11010-007-9478-6

21. Gertler AA, Cohen HY (2013) SIRT6, a protein with many faces. Biogerontology 14 (6):629-639. doi:10.1007/s10522-013-9478-8

22. Li X (2013) SIRT1 and energy metabolism. Acta biochimica et biophysica Sinica 45 (1):51-60. doi:10.1093/abbs/gms108

23. Laurent G, German NJ, Saha AK, de Boer VC, Davies M, Koves TR, Dephoure N, Fischer F, Boanca G, Vaitheesvaran B, Lovitch SB, Sharpe AH, Kurland IJ, Steegborn C, Gygi SP, Muoio DM, Ruderman NB, Haigis MC (2013) SIRT4 coordinates the balance between lipid synthesis and catabolism by repressing malonyl CoA decarboxylase. Molecular cell 50 (5):686-698. doi:10.1016/j.molcel.2013.05.012

24. Horio Y, Hayashi T, Kuno A, Kunimoto R (2011) Cellular and molecular effects of sirtuins in health and disease. Clinical science 121 (5):191-203. doi:10.1042/CS20100587

25. Mishra J, Singh S (2013) Miltefosine resistance in Leishmania donovani involves suppression of oxidative stress-induced programmed cell death. Experimental parasitology 135 (2):397-406. doi:10.1016/j.exppara.2013.08.004

26. Merksamer PI, Liu Y, He W, Hirschey MD, Chen D, Verdin E (2013) The sirtuins, oxidative stress and aging: an emerging link. Aging 5 (3):144-150

27. Choi JE, Mostoslavsky R (2014) Sirtuins, metabolism, and DNA repair. Current opinion in genetics & development 26:24-32. doi:10.1016/j.gde.2014.05.005

28. Cheung KG, Cole LK, Xiang B, Chen K, Ma X, Myal Y, Hatch GM, Tong Q, Dolinsky VW (2015) Sirtuin-3 (SIRT3) Protein Attenuates Doxorubicin-induced Oxidative Stress and Improves Mitochondrial Respiration in H9c2 Cardiomyocytes. The Journal of biological chemistry 290 (17):10981-10993. doi:10.1074/jbc.M114.607960

29. McDonnell E, Peterson BS, Bomze HM, Hirschey MD (2015) SIRT3 regulates progression and development of diseases of aging. Trends in endocrinology and metabolism: TEM 26 (9):486-492. doi:10.1016/j.tem.2015.06.001

30. Dryden SC, Nahhas FA, Nowak JE, Goustin AS, Tainsky MA (2003) Role for human SIRT2 NAD-dependent deacetylase activity in control of mitotic exit in the cell cycle. Molecular and cellular biology 23 (9):3173-3185

31. Kilic Eren M, Kilincli A, Eren O (2015) Resveratrol Induced Premature Senescence Is Associated with DNA Damage Mediated SIRT1 and SIRT2 Down-Regulation. PloS one 10 (4):e0124837. doi:10.1371/journal.pone.0124837

32. Cea M, Soncini D, Fruscione F, Raffaghello L, Garuti A, Emionite L, Moran E, Magnone M, Zoppoli G, Reverberi D, Caffa I, Salis A, Cagnetta A, Bergamaschi M, Casciaro S, Pierri I, Damonte G, Ansaldi F, Gobbi M, Pistoia V, Ballestrero A, Patrone F, Bruzzone S, Nencioni A (2011) Synergistic interactions between HDAC and sirtuin inhibitors in human leukemia cells. PloS one 6 (7):e22739. doi:10.1371/journal.pone.0022739

33. Sonnemann J, Marx C, Becker S, Wittig S, Palani CD, Kramer OH, Beck JF (2014) p53-dependent and p53-independent anticancer effects of different histone deacetylase inhibitors. British journal of cancer 110 (3):656-667. doi:10.1038/bjc.2013.742

34. Peck B, Chen CY, Ho KK, Di Fruscia P, Myatt SS, Coombes RC, Fuchter MJ, Hsiao CD, Lam EW (2010) SIRT inhibitors induce cell death and p53 acetylation through targeting both

SIRT1 and SIRT2. Molecular cancer therapeutics 9 (4):844-855. doi:10.1158/1535-7163.MCT-09-0971

35. Ouaissi A (2003) Apoptosis-like death in trypanosomatids: search for putative pathways and genes involved. Kinetoplastid biology and disease 2 (1):5. doi:10.1186/1475-9292-2-5

36. Williams RA, Smith TK, Cull B, Mottram JC, Coombs GH (2012) ATG5 is essential for ATG8-dependent autophagy and mitochondrial homeostasis in Leishmania major. PLoS pathogens 8 (5):e1002695. doi:10.1371/journal.ppat.1002695

37. Gal J, Bang Y, Choi HJ (2012) SIRT2 interferes with autophagy-mediated degradation of protein aggregates in neuronal cells under proteasome inhibition. Neurochemistry international 61 (7):992-1000. doi:10.1016/j.neuint.2012.07.010

38. Sengupta S, Chowdhury S, Bosedasgupta S, Wright CW, Majumder HK (2011) Cryptolepine-Induced Cell Death of Leishmania donovani Promastigotes Is Augmented by Inhibition of Autophagy. Molecular biology international 2011, article ID 187850, doi:10.4061/2011/187850

Figure Legends.

Figure 1. Molecular structure of the KH-TFMDI, an 3-arylideneindolin-2-one compound.

Figure 2. Growth curves of *Leishmania amazonensis* promastigotes **(A)** and intracellular amastigotes **(B)** treated with different concentrations of KH-TFMDI. For the promastigotes, KH-TFMDI was added after 24 h of growth (arrow). For intracellular amastigotes, macrophages were firstly infected with metacyclic promastigotes and then after 24 h of infection, different concentrations of KH-TFMDI were added and the cells were monitored for up to 72 h. Three independent experiments were performed; each bar represents the standard deviation. Asterisks mean different degrees of significance between treated groups and the control. *p* values: * $p<0.02$; ** $p<0.002$; *** $p<0.0002$.

Figure 3. Phase contrast microscopy and immunofluorescence microscopy with 3D deconvolution of *Leishmania amazonensis* promastigotes using anti-α-tubulin antibody and DAPI. **(A-B)** Control parasites; **(C-D)** 3 μM KH-TFMDI; **(E-F)** 5 μM KH-TFMDI. For both concentrations of KH-TFMDI, the treatment duration was 24 h. The green labeling corresponds to the cytoskeleton, mainly comprised of subpellicular microtubules. The blue DAPI labeling corresponds to the kinetoplasts. After treatment with KH-TFMDI, the promastigotes became thinner and more elongated when compared with the control parasites. The arrowheads in the fluorescence images point to some cells that presented significant alterations in the morphology.

Figure 4. Scanning electron microscopy of *Leishmania* amazonensis promastigotes **(A)** Control parasites after 72 h of growth; parasites treated with 3 μM KH-TFMDI **(B,C,F)** or 5 μM **(D-E)** 10 μM KH-TFMDI for 48 h. KH-TFMDI induced dramatic and significant alterations in the shape of the promastigotes. Several cells were swollen at the anterior/medial region of the body where the nucleus is located (arrowhead), and then the cell bodies became thinner and elongated. In many treated cells, blebs also appeared in the cell body (arrows).

Figure 5. Morphometric analysis of *Leishmania amazonensis* promastigotes after exposure to KH-TFMDI. **(A-B)** Scanning electron microscopy of a control **(A)** and a promastigote treated with 5 μM KH-TFMDI for 48 h. **(C-D)** Fluorescence microscopy of Hoescht-labeled control **(A)** and a promastigote treated with 5 μM KH-TFMDI for 48 h. **(E-I)** Graphic analysis of the cell body area, cell and flagellum length and distance between nucleus and kinetoplast obtained by measurement of several cells using the NIH Image J Software. All the measurements confirm the morphological alterations induced by the treatment, where the promastigotes became thinner and elongated changing the area of cell body and the length of the flagellum.**(panel I)**. **(J)** Table summarizes the mean number of measurements for the control and 5 μM KH-TFMDI treated-promastigotes.

Figure 6. Differential interferencial contrast (DIC) microscopy and immunofluorescence of *Leishmania amazonensis* promastigotes with anti-acetylated tubulin antibody and DAPI. **(A-B)** Control parasites; **(C-D)** 3 μM KH-TFMDI; **(E-F)** 5 μM KH-TFMDI. For both concentrations, the treatment duration was 48 h. The images suggest a concentration-dependent accumulation of acetylated-tubulin in response to KH-TFMDI, indicating an inhibition of HDAC and tubulin hyperacetylation.

Figure 7A-I. Detection of acetylated tubulin and α-tubulin in KH-TFMDI-treated *Leishmania amazonensis* promastigotes by Western blot, densitometry and flow cytometry. **(A)** The SDS-PAGE gel was stained with Pounsor; equal amounts of protein were loaded in all the lanes. Immunoblotting using **(B)** anti-acetylated tubulin antibody or **(C)** anti-α-tubulin antibody. **(D)** Measurement of the area related to the labeling of the SDS-Page gel with Pounsor. Densitometry analysis of the anti-acetylated tubulin **(E)** and anti-α-tubulin **(F)** labeling. The values of the areas plotted on the graphs indicate that there is a 4.54% and 8.84% increase in the acetylation of tubulin in response to treatment with 3 μM and 5 μM TFMDI, respectively. **(F)** There was also an increase in the amount of α-tubulin after treatment with 3 μM

TFMDI; however, the increase is not significant. **(G-I)** Flow cytometry analysis of tubulin acetylation of control and KH-TFMDI-treated promastigotes to confirm the results obtained by western blotting and densitometry analysis. The increase in the tubulin acetylation was concentration-dependent when parasites were treated with 3 and 5 µM after 48 h of treatment.

Figure 8. Ultrathin sections of *Leishmania amazonensis* promastigotes treated with KH-TFMDI. **(A)** Control parasite after 72 h of growth; **(B-D)** parasites treated with 5 µM KH-TFMDI for 48 h; **(E)** parasite treated with 10 µM KH-TFMDI for 48 h. The images suggest the formation of blebs in the plasma membrane that covers the cell body (C, arrowhead). In Figure 7B, the arrow points to the presence of a lipid body in the same location as the blebs. Panels D and E show parasites displaying several morphologically distinct lipid bodies randomly distributed throughout the cytoplasm, some of them near a mitochondrial profile that is completely altered (Fig. D, small arrow). Panel E shows mitochondrial swelling, loss of the matrix content and vesiculation of the inner mitochondrial membrane (arrowhead). F, flagellum; k, kinetoplast; LB, lipid body; M, mitochondrion; N, nucleus.

Figure 9. Ultrathin sections of *Leishmania amazonensis* promastigotes treated with KH-TFMDI**.** The parasites were treated with 10 µM KH-TFMDI for 48 h. Panel A shows a endoplasmic reticulum profile surrounding parts of the cytoplasm, lipid bodies (arrows) and a glycosome (arrowhead). In this image, we also observe several small vesicles inside flagellar pocket. Significant alterations were observed in the nucleus including chromatin decondensation **(B)** or fragmentation **(C-F)**; deformation of the cell body **(B-D, small arrows)**; mitochondrial lesions **(D,F, arrowhead)**; and, close association of lipid bodies with plasma membrane and mitochondrion **(A,D,F, arrows)**. FP, flagellar pocket; k, kinetoplast; LB, lipid body; M, mitochondrion; N, nucleus.

Figure 10. Cytochemical analysis with phosphotungstic acid (PTA) of *Leishmania amazonensis* promastigotes treated with KH-TFMDI. **(A)** Control parasite after 72 h of growth; **(B-C)** parasites treated with 5 µM KH-TFMDI for 48 h; **(D)** parasites treated with 10 µM KH-TFMDI for 48 h. All images suggest significant alterations in the pattern of chromatin condensation induced by KH-TFMDI (B-D) that is absent in control parasite (A). Panel B shows a treated-promastigote where the nuclear matrix appears completely electron lucent indicating loss of chromatin condensation, while panel C indicate that

there are condensed and decondensed chromatin after treatment (arrow). On the other hand, panel D show an intense chromatin fragmentation.

Figure 11. Evaluation of different cellular phenotypes induced by KH-TFMDI on *Leishmania amazonensis* promastigotes: lipid bodies accumulation, cell viability, oxidative stress and mitochondrial function. **(A)** Effects of KH-TFMDI on the accumulation of lipid bodies using Nile Red, a marker for neutral lipids. The analysis showed a concentration-dependent effect that is significant at both KH-TFMDI concentrations used. **(B)** Evaluation of plasma membrane integrity using propidium iodide by flow cytometry. Results indicate a reduction of 25% of the cell viability at concentration of 5µM of KH TFMDI for 72 h of treatment. P values: *p<0;01; ***p<0.001. **(C)** Analysis by MTS assay. Using this method, the results were completely different; we observed a reduction of 75% of the cell viability after treatment with 5µM KH TFMDI for 72 h. *p* values: *p<0.03; **p<0.003; P values: ** p<0.01; ***p<0.001, ****p<0.0001; **(D-F)** Evaluation of the oxidative stress by production of ROS and mitochondrial superoxide. KH-TFMDI induced an increase of 17% and 35% in the ROS production after treatment with 5 µM for 24 h **(Panel C)** and 48 h **(Panel D)**, respectively. *p* values: *p<0.01, ***p<0.001, ***p<0.001; **(F)** Treatment with 5 µM KH-TFMDI for 48 h also induced an increase of mitochondrial superoxide in 18% when compared with control parasites. *p* values: *p<0.01 ***p<0.001, ***p<0.001. **(G-H)** Evaluation of the mitochondrial transmembrane potential (ΔΨ*m*) using JC1 marker after treatment with different concentrations of KH-TFMDI for 48 h. KH-TFMDI induced a collapse in the ΔΨ*m* similar to those obtained with FCCP.

Figure 12. Analysis of the cell cycle using propidium iodide by flow citometry. *Leishmania amazonensis* promastigotes were treated with different concentrations of KH-TFMDI for 24 **(A)**, 48 **(B)** and 72 h **(C)**. After 24h of treatment, a significant increase in population of cells in G0/G1 were observed with 4 and 5 µM KH-TFMDI **(A)**. This increase is more significant after 48h **(B)**. After 72 h, around 60% of the population was found in G0/G1 phase, however a significant increase of the population in sub-G0 was also observed, indicating the presence of parasites undergoing cell death. In addition, a decrease in population in G2/M phase was observed, confirming the arrest of cell cycle in G0/G1. *p* values: *p<0.05, **p<0.01, ***p<0.001, ****p<0.0001.

Figure 13. Analysis of DNA fragmentation in *Leishmania amazonensis* promastigotes after treatment with KH-TFMDI for 48 h. **(A)** Control parasite after 72 h of growth; **(B)** parasites treated with 3 μM KH-TFMDI for 48 h; **(C)** parasites treated with 4 μM KH-TFMDI for 48 h; **(D)** parasites treated with 5 μM KH-TFMDI for 48 h; **(E)** parasites treated with 10 μM KH-TFMDI for 48 h. A significant increase in DNA fragmentation was observed for the concentrations of 3, 4 and 5 μM; for 10 μM, a significant reduction was observed and may be related to total destruction of the parasites.
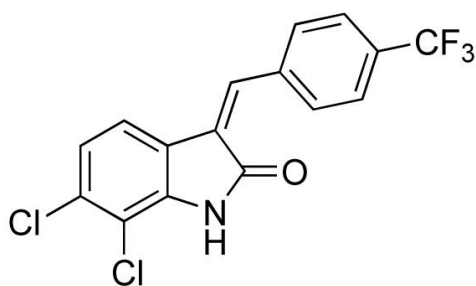
Figure 1.

Table 1. Summary of the IC$_{50}$ values found for KH-TFMDI during the treatment of promastigotes and intracellular amastigotes forms of *Leishmania amazonensis*. The IC$_{50}$ was calculated as described in the methodology section.

	IC$_{50}$ values (µM)		
Time of incubation	**24h**	**48h**	**72h**
Promastigotes	2,376	2,438	1,976
Intracellular amastigotes	4,735	2,341	1,148